Physics PhD Thesis Proposal

Dynamic Resonance Calibration for Advanced Gravitational Wave Detectors

Student: H. Pablo Daveloza

Advisor: Mario Diaz

Mentors: Richard Savage / Jeffrey Kissel

LIGO Document DCC-T1400202

March 31, 2014

1 Introduction

The "observation" of Gravitational Wave (GW) is one of the most important scientific challenges of our time. Their detection will open a new window to explore astrophysical events, some of them inaccessibles through electromagnetic observation alone. The importance of GW observations comes from open questions that could be answered, or at least constrained, by them. For example: "properties of the equation of states of high-density matter, as in the cores of Neutron Stars (NS), are still incompletely known, because the physical conditions are not directly accessible by experiments", measurement of GW ring-down of a binary system of NSs will constrain the NS equation of state [1], while confirming theoretical mechanisms of formation of coalescing of binary systems [2]. Also, GW will test General Relativity in the strong-field regime [3][4], and will set new boundaries for values of cosmological parameters like the Hubble constant for example [5][6].

As is well state it by Salvatore Vitale, et a. [7]: "In order to extract as much physical information as possible, all the known sources of error must be eliminated, reduced or quantified". Due to the inability of producing our own GW[1], the calibration of GW detectors relies on a set of different measurements. The uncertainties in these measurements not only determine the accuracy to which one may compare a given detector's output with another, but also constrains the reconstruction of a possible gravitational wave form, which in turns, affects the accuracy to determine parameters from the astrophysical source, like masses, sky location, distance, inclination and orientation.

Nowadays, GW detectors like LIGO and Virgo are being upgraded to reach sensitivities of $\sim 10^{-23}\ m$. Within the upgrades, new actuators, optics, electronics, etc, introduced new challenges for the calibration of these new instruments. This proposal focuses in one of the calibration technique based on dynamic resonance [8], usually called Voltage Controlled Oscillator (VCO). The following chapter will introduce the basic ideas of LIGO calibration, and will explore the limits and possibles different applications of VCO for the new generation of GW interferometers, with the prospect of achieving the finest accuracy within our possibilities.

1.1 Gravitational Waves

In 1916 Albert Einstein presented a paper called "*Approximative Integration of the Field Equations of Gravitation*" [9]. The paper shows the possible existence of a metric perturbation which propagates like a wave, what today is called a gravitational wave. Since then, many articles had study and going deeper into the subject. This proposal will not intend to summarizes all the work done about GW. A good starting point for the interest reader is REFERENCIAS!. In this chapter, I present some simple ideas that will help the reader to understand why interferometry is used in GW detection.

Albert Einstein, after explaining the "apparent" contradiction of Fizeau and Michelson-Morley experiments by his theory of special relativity, went several step forward with his theory of General Relativity. The main distinction between those two theories is a "matter of matter". General Relativity introduces the idea of gravity as a deformation of our four dimensional space-time arena produced by mass; meanwhile, special relativity takes place in what is usually called flat, Minkowski, non deform by mass, space-time. Gravitational Waves appears as a special solution of Einstein's equation:

$$R_{ab} - \frac{1}{2} R\ g_{ab} = -8\pi\ T_{ab} \tag{1}$$

In the equation, T_{ab} is the energy-momentum tensor which contains information about the astrophysical source, its mass for example; the metric, g_{ab}, relates the length and time between points in the space-time, which depends on the path; finally, R_{ab} and R are the Ricci tensor and Ricci scalar respectively, they are the sum of derivatives and contractions of the metric. From a basic point of view, the equation is the relation between mass (T_{ab}) and the deformation of the path (g_{ab}).

[1] Strong enough to be detected by our instruments.

In the *Weak Field Approximation*, the metric can be expressed as a perturbation, $h_{\mu\nu}$, of the flat Minkowski metric, $\eta_{\mu\nu}$, such as $g_{\mu\nu} = \eta_{\mu\nu} + h_{\mu\nu}$. In this approximation, Einstein's equation becomes

$$\Box\bar{h}^{\mu\nu} = \left(-\frac{1}{c^2}\frac{\partial^2}{\partial t^2} + \nabla^2\right)\bar{h}^{\mu\nu} = -16\pi T^{\mu\nu} \tag{2}$$

Far away from the source where $T^{\mu\nu} = 0$, one possible solution for $\bar{h}^{\mu\nu}$ is a propagating wave, a gravitational wave.

There is some freedom on how express the metric perturbation. A particularly useful one is the transverse-traceless (TT) gauge, in which $h^{\mu\nu}$ can be expressed as the sum of two independent "polarizations", $h^{\mu\nu} = h_+^{\mu\nu} + h_x^{\mu\nu}$, where $h_+^{\mu\nu}$ is called plus polarization, and $h_x^{\mu\nu}$ cross polarization. The choice of this gauge make it easy to visualize how an interferometer could be uses as a GW detector. The following schematic, Figure 1, shows the effect of a plus polarize GW passing through a ring of free masses, expanding and contracting the circle in perpendicular directions. If the free masses were the mirrors of a Michelson interferometer, then the interference pattern can be used as a GW detector.

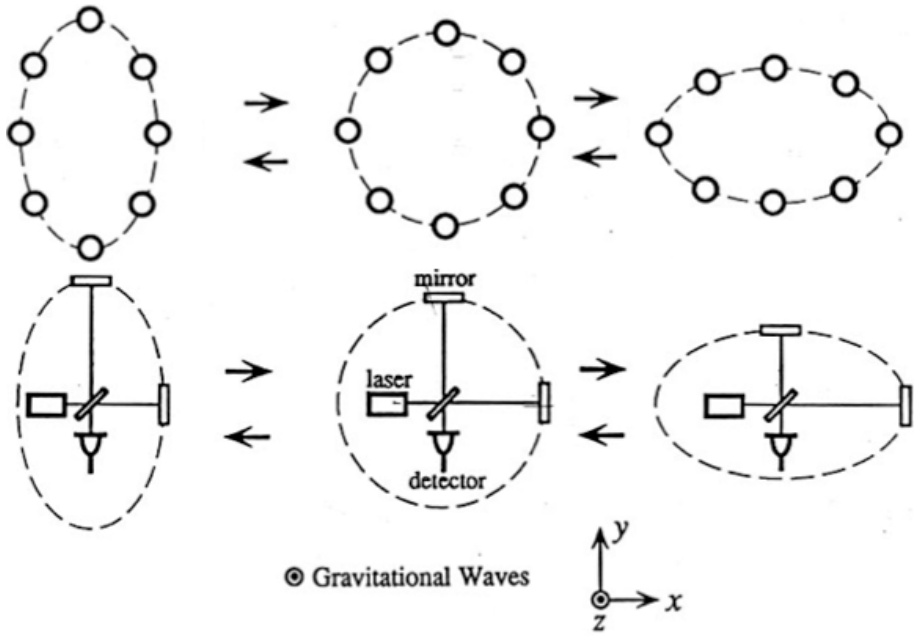

Figure 1: Plus polarization GW effect on free masses (top), and the effect on "free mirrors" of a Michelson interferometer (bottom). (*Credit: J. Kissel*)

.

2 Detection

No one has ever detected directly gravitational waves, and their very existence was in doubt until 1981 when Taylor and Weisberg showed that the binary pulsar PSR 1913+16 was losing energy in a rate that matched the calculations based on general relativity GW emissions [10]. Nowadays, cosmic microwave background observation by BICEP2 collaboration [11], showed the importance of primordial gravitational waves in the beginning of times. In years to come, direct detection of GW from the most violent astrophysical events will expand the knowledge of our own universe.

2.1 Resonant Bars

GW are small ($|\bar{h}^{\mu\nu}| = h \sim 10^{-23}$) perturbations of the space-time fabric which makes their detection very difficult. In 1950s, Weber built the first detector for gravitational waves. It was an aluminum cylinder with piezo-electric transducers attached to its sides, commonly known today as Resonant Bar detector [12] [13]. In 1969 Weber announced that two of his bar detectors, separated by a few hundred miles, were excited simultaneously by a gravitational wave passing the earth [14]. In the following years other research groups repeated Weber's experiment but failed to detect anything. Nonetheless, Weber's pioneering work inspired many physicists, and by 1980 there were several detectors similar to that of Weber operating around the world.

2.2 Interferometers

The idea of using interferometry to sense gravitational waves is almost as old as the idea of using a resonant bars. It was independently suggested by several physicists, among them are Gertsenshtein and Pustovoit [15], Weber [16], and Weiss [17]. The first interferometer for gravitational-wave detection was built by Forward [18] at Hughes Research Laboratories in Malibu, California in 1971.

In the simplest scenario shown in Figure 1, where the polarization is aligned with the interferometer's arms, and using the long wavelength approximation (the perturbation is assumed constant along the arm), the gravitational wave strain amplitude, $h(t)$, can be expressed as

$$h(t) = \frac{L^x_{ext}(t) - L^y_{ext}(t)}{L} = \frac{\Delta L_{ext}(t)}{L} \tag{3}$$

where $L^{x,y}_{ext}$ is the actual length of the X or Y interferometer's arm, meanwhile L is the mean value of them. The difference, ΔL_{ext}, is called external differential arm (DARM) length change.

In the frequency domain, $\Delta L_{ext}(f)$ is measured using interferometry by monitoring the differential phase between light returned by each cavity giving rise to a digital DARM error signal. Under servo control the error signal, $e_D(f)$, is proportional to $\Delta L_{ext}(f)$ such that

$$\Delta L_{ext}(f) = R_L(f) \times e_D(f) \tag{4}$$

where the change in length ΔL_{ext}, actually, is the sum of the interferometer's response to astrophysical signal and other external noise sources. $R_L(f)$ is a complex function called "length response function".

As one can see from equation 3, ΔL_{ext} is proportional to the path length L, which explain why GW interferometers like LIGO and VIRGO have kilometers long arms. Nevertheless, even with kilometer scale arms, the photon transit time is short, making GW observations difficult. To mend this, GW interferometers utilizes Fabry-Perot cavities which makes the photon transit time proportional to the cavity finesse.

Each LIGO detector is a Signal-recycled Power-recycled Fabry-Perot Michelson interferometer. Basically, a Michelson interferometer where Fabry-Perot cavities are annexed to the end of each arm. In addition two extra cavities are annexed, one at the laser input and the other at the Michelson output, creating the Power-recycled and Signal-recycled cavities, see Figure 2.

In order to operate a dual-recycled Fabry-Perot Michelson interferometer, all cavities must remain in resonance, meanwhile each mirror should behave as a "free mass". To achieve this, and also the required sensitivity, each mirror should be seismically isolated. The LIGO community designed and constructed a specific suspension and control system for the Fabry-Perot cavity mirrors. Part of this system is a "Quadruple-Suspension", Figure 3. The Quadruple-Suspension, as its name suggest, has four stages where each of them is controlled independently with a set of magnet and coil actuator[2]. The calibration and characterization of these actuator are the most important part of LIGO calibration.

The complexity of the stabilization, control, seismic isolation, etc, of the complete interferometer is the immense work of the LIGO community, which consists of more than 900 scientist

[2]Actually, the last stage of the suspension uses a system based on electrostatic actuator called Electrostatic Drive or ESD.

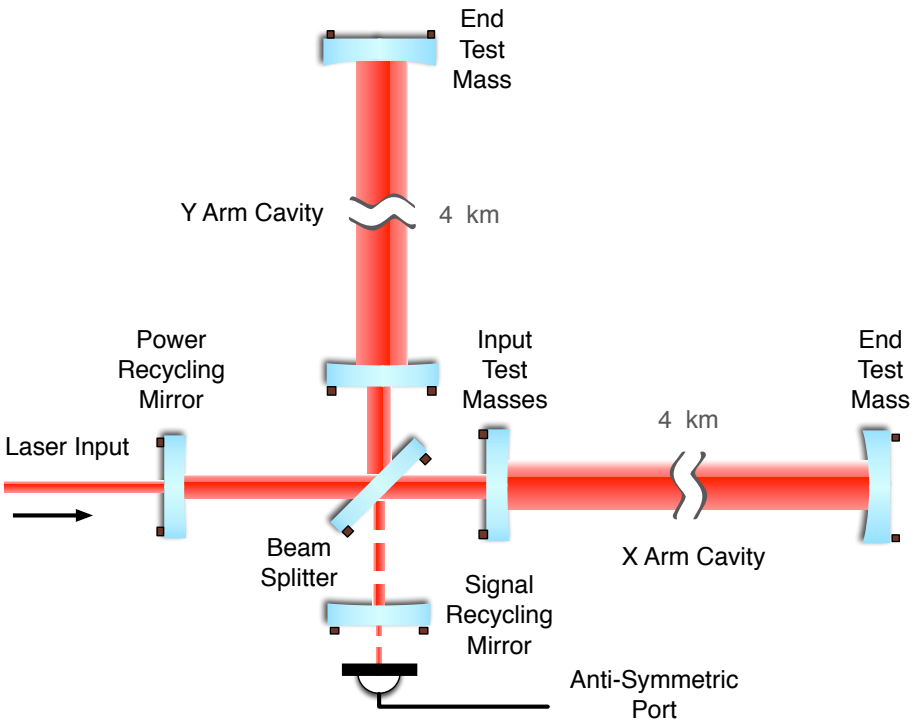

Figure 2: Signal-recycled Power-recycled Fabry-Perot Michelson interferometer. (*Credit: J. Kissel schematic*)

in more than 13 institutions around the world. Fortunately, this proposal focus only in the calibration of the interferometer. The following chapters will explain the general concepts of LIGO calibration, particularly, the calibration of the actuation function of the mirror suspension system, Quadrupole-Suspension, through an specific technique, the VCO calibration.

3 LIGO Calibration

The goal of LIGO calibration is to reconstruct, as accurate as possible, the relative displacement sensed by the arms of the interferometer in order to perform GW searches, which in an abuse of notation, we will express it as $h(t)$. The calibration relies on the DARM error signal, $e_D(f)$, and the response function, $R_L(f)$, to calculate $h(t)$ within certain accuracy.

The calibration is a dynamic procedure that can be separated into three main sections:

- Frequency Domain: calculation of the interferometer's frequency domain response function, $R(f)$, based on a set of measurements of specific parameters, scaling factors, and digital filters.
- Time Domain: generation of the LIGO strain data stream, $h(t)$, based on the frequency domain model. The strain data stream is where GW searches are performed.
- Error Budget: response function's uncertainty, which affects the accuracy to determine parameters of astrophysical sources.

Errors in the time domain calculation are smaller compared to the ones of the frequency domain model [20][21], therefore, the rest of the document will focus on the frequency domain calibration.

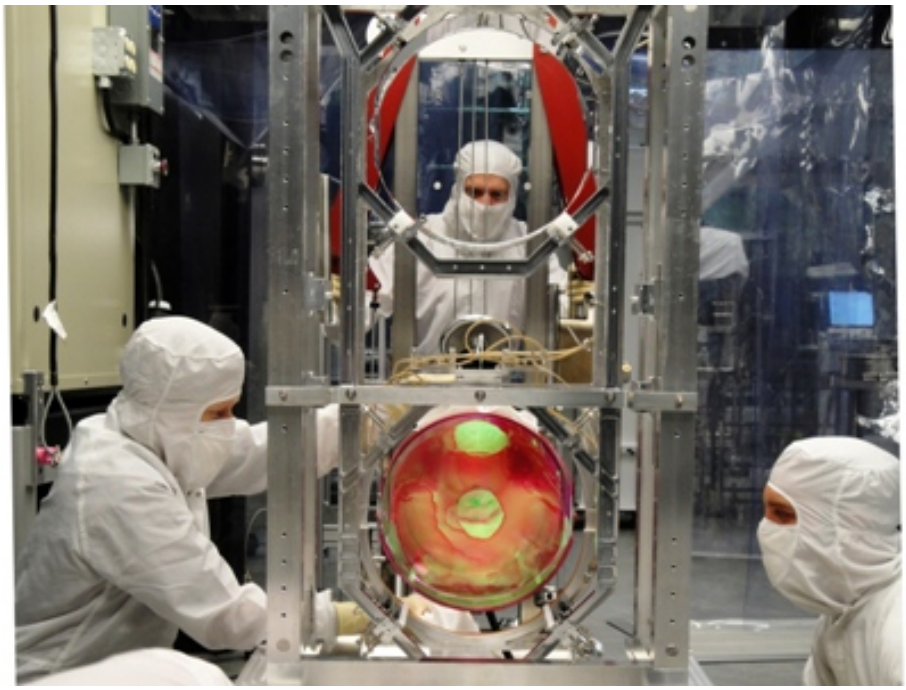

Figure 3: Advanced LIGO Large Optics Suspension, (*http://www.ligo.org/multimedia/gallery/opt.php*).

3.1 Frequency Domain Calibration

The feedback control system that keeps cavities on resonance (and therefore, ΔL_{ext} proportional to e_D) is modeled, Figure 4, as a single-input, single-output control loop with three main subsystems

- $C_L(f,t) = \gamma(t)C_L(f)$: the *length sensing function*, which describes how the interferometer responds to DARM variations.
- $D(f)$: a set of *digital filters* used to shape the loop error signal into a control signal.
- $A(f)$: the *actuation function*, which describes how the Fabry-Perot end mirror, also called End Test Mass (ETM), physically respond to the digital control signal.

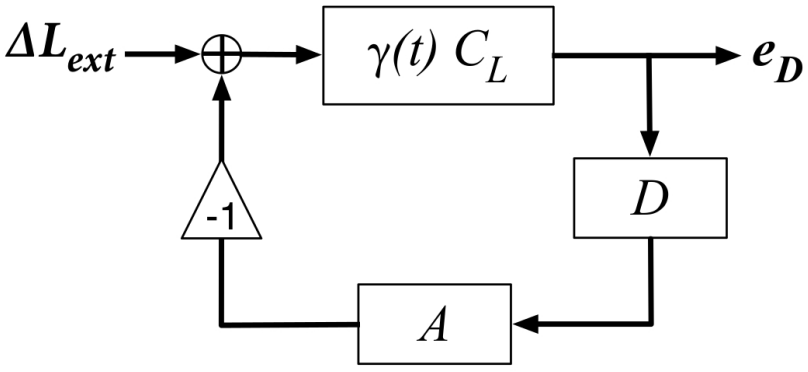

Figure 4: The single-input, single-output model of the calibration control loop.

The response function can be derived from Figure 4 and Equation 4 as

$$R_L(f,t) = \frac{1+\gamma(t)\ C_L(f)D(f)A(f)}{\gamma(t)C_L(f)} = \frac{1+\gamma(t)G_L(f)}{\gamma(t)C_L(f)} \tag{5}$$

where $G_L(f) \equiv C_L(f)D(f)A(f)$ is the "open loop transfer function".

3.1.1 Sensing Function

The sensing function is affected by a slow time-dependence of the optical gain produced by small, low-frequency ($f \ll 40Hz$) alignments and thermal lensing fluctuations in the resonant cavities. These effects are modeled as an independent function $\gamma(t)$, in such a way that the sensing function can be expressed as

$$C_L(f,t) = \gamma(t)C_L(f) \tag{6}$$

The frequency-dependent part, $C_L(f)$, is modeled as

$$C_L(f) = \mathcal{K}_C \times C_{FP}(f) \times ADC(f) \tag{7}$$

where $ADC(f)$ represents the frequency dependence of the anti-aliasing filters and digitization process. $\mathcal{K}_C$ absorbs all proportionality constants and dimensions of the sensing process. Finally, $C_{FP}(f)$ is the sum of the X-Y Fabry-Perot cavitiy responses [20], where each one can be expressed as

$$H_{FP}(f) = \frac{2\pi}{\lambda}\frac{r_e(1-r_i^2)}{(r_i-r_e)}\frac{\sin(2\pi fL/c)}{2\pi fL/c}\frac{e^{-2\pi ifL/c}}{1-r_ir_ee^{-4\pi ifL/c}} \tag{8}$$

where λ is the laser wavelength, r_i and r_e are the amplitude reflectivity of the Input Test Mass and ETM of the Fabry-Perot cavity, and c is the speed of light. In the frequency range where $f \ll 2c/L$, the frequency-dependence of $H_{FP}(f)$ can be approximated by a simple "cavity pole" transfer function, $H_{SP}(f) = (1+if/f_c)^{-1}$, such that

$$C_{FP}(f) \approx H_{SP}^x(f) + H_{SP}^y(f) \tag{9}$$

where $H_{SP}^{x,y}$ represent the response of the X or Y Fabry-Perot arm cavity.

3.1.2 Digital Filters

$D(f)$ is a set of compensation filters, used to shape the error signal $e_D(f)$ into a control signal $s_D(f)$, see Figure 5. These filters are completely known, adding no uncertainty to the model.

3.1.3 Actuation Function

The actuation function is described as a linear combination of the X and Y ETM functions

$$A(f) = \xi^x A^x(f) + \xi^y A^y(f) \tag{10}$$

where $\xi^{x,y}$ are known digital coefficients of order unity and opposite in sign. $A^{x,y}(f)$ is the individual ETM actuation functions modeled as

$$A^{x,y}(f) = \mathcal{K}_A^{x,y} \times [D_A^{x,y}(f) \times DAC(f) \times P^{x,y}(f)] \tag{11}$$

For each arm, the control signal $s_D(f)$ passes through digital suspension filters, $D_A^{x,y}(f)$, converted from a digital signal to an analog voltage via the digital to analog conversion element $DAC(f)$, which includes analog anti-imaging circuitry. The resulting voltage is converted into current, and it is sent to the coil actuators and/or ESD which convert the current into force on the suspension system. The suspended test mass is displaced according to the force-to-displacement transfer function, $P(f)$, changing each arm cavity length. All dimensions and frequency-independent factors in the actuation path are included in $\mathcal{K}_A$.

In the past, mirrors were suspended as a simple pendulum. Therefore, the force-to-displacement model was expressed as

$$P(f) \propto \frac{1}{[f_0^{cm}]^2 + i\frac{f_0^{cm}}{Q^{cm}}f + f^2} \tag{12}$$

where f_0^{cm} and Q^{cm} are the frequency and quality factor of the pendulum.

In the current configuration, mirrors are suspended by the Quadruple-Suspension system. The complexity of this suspension system leads to a complicated Simulink model [19] for the force-to-displacement transfer function. The application of this model to the calibration is a work in progress.

4 Measurements

Even when the following chapter is mostly based on the calibration of LIGO Fifth Science Run (S5) [20], results are general and can be applied to second generation of GW interferometers, like Advanced LIGO.

In order to calculate the response function $R_L(f)$, measurements of specific parameters from the actuation and sensing function are needed. Digital filters are completely known, and are included without uncertainty. All the parameters mentioned in the previous chapter were measured or estimated, however, several are derived from measurements with negligible uncertainty, or little effect in the frequency band of interest ($10Hz \leq f \leq 6kHz$). This chapter will focus on those relevant quantities for the calculation of the response function uncertainty, $\mathcal{K}_C$, $\mathcal{K}_A$, $G_L(f)$, and $\gamma(t)$ [20][21].

The magnitude of $\mathcal{K}_C$ cannot be measure without servo control, so, it is estimated as the ratio of the model and measurements of the open loop transfer function $G_L(f_{UGF})$[3].

$$\mathcal{K}_C = \frac{G_L(f_{UGF})}{A(f_{UGF}) \times D(f_{UGF}) \times [C_{FP}(f_{UGF}) \times ADC(f_{UGF})]} \tag{13}$$

This estimation, makes $\mathcal{K}_A$ measurements crucial, since they set the frequency-independent magnitude of the entire response function.

Finally, continuous measurements of $\gamma(t)$ track the time dependence of the response function.

4.1 Time Dependence, $\gamma(t)$

The time dependence of the sensing function is measured by digitally injecting a signal, $s_{cl}(f)$ on Figure 5, at the output of the digital filters, $D(f)$, prior to the control signal, $s_D(f)$, at three frequencies f_{cl} near 50, 400, and 1100 Hz.

From Figure 5, the time-dependent coefficient $\gamma(t)$ can be derived as

$$\gamma(t) = -\frac{1}{G_L(f_{cl})}\frac{s_D(f_{cl}) - s_{cl}(f_{cl})}{s_D(f_{cl})} \tag{14}$$

where $G_L(f_{cl})$ is the modeled DARM open loop transfer function at the reference time at a given calibration line frequency, f_{cl}. The coefficient generated from $f_{cl} \approx 400$ Hz is used to scale the response function model; the other two frequencies are used to confirm that the variations are independent of frequency.

4.2 Sensing Scaling Coefficient, $\mathcal{K}_C$, and Open Loop Transfer Function, $G_L(f)$

In order to estimate $\mathcal{K}_C$, a frequency-dependent open loop model is developed using the remainder of the sensing subsystem, scaled by the measured actuation and the known digital filter gain.

[3] f_{UGF} is the unity gain frequency of the DARM control loop

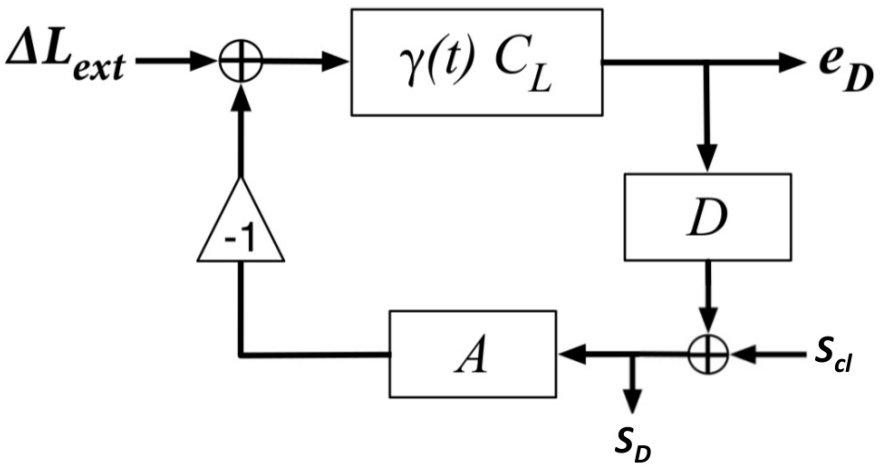

Figure 5: Calibration control loop with calibration (s_{cl}) and control (s_D) signals.

The open loop transfer function, $G_L(f)$, is measured while the interferometer is controlled, operating in the nominal configuration, at designed sensitivity. During the measurement, $\gamma(t)$ is set equal to 1. This measurement is compared against the model of the open loop transfer function and the model scaled by the measurement's magnitude to form $\mathcal{K}_C$.

4.3 Actuation Scaling Coefficients, $\mathcal{K}_A^{x,y}$

The standard method for determining the actuation coefficients, $\mathcal{K}_A^{x,y}$, is known as the "Free-Swinging Michelson" technique (MITCH) [20][21]. The method uses the interferometer's well-known Nd:YaG[4] main laser wavelength ($\lambda = 1064.1 \pm 0.1$nm) as the calibrated length reference while using the test mass coil actuators to cause a length change. This method goes through a series of steps, calibrating first the Input Test Masses actuators, and then using these measurements to calibrate the ETM actuators. Sequential measurements in different interferometer and electronics configuration, increases the sources of systematics errors. The order of magnitude of displacement produced by MITCH are of $\sim 10^{-8}m$, which implies extrapolation over nearly 12 orders of magnitude in actuation range. During S5, estimated errors for MITCH were approximately 10% [22].

Another calibration method is the Photon calibrator or Pcal [23]. Pcal uses photon pressure over the ETMs to produce a calibrated displacement through the power modulation of auxiliary lasers. This method is, until today, the only calibration method that can be used during the interferometer most sensitive configuration called science mode. Displacement of $\sim 10^{-22}m$ are expected using this method, which are the expected order of magnitude for GW. The primary identified sources of systematic error for Pcal are rotation due to beam centering offsets and absolute power calibration of the auxiliary lasers. It was shown [22] that uncertainties of 1% or less are achievable with this method.

During S5, a third technique was tested. The method, based on dynamic resonance (see 6.1), is called "Laser Frequency Modulation", or also "Voltage-Controlled Oscillator" (VCO) [24]. The method produces a calibrated variation of the cavity length through a controlled modulation of the main laser's frequency. Since VCO varies the main laser's frequency, is not possible to produce a DARM signal because is a common mode of the interferometer. Therefore, one should calibrate one arm at a time, and is not possible to apply VCO in science mode. Cavity's length variation of $\sim 10^{-13}m$ where possible during S5. VCO relies on accurate measurement of the sideband-to-carrier ratios and extrapolation over approximately 5 orders of magnitude in actuation range. Another inconvenient is the low SNR product of a Input Mode Cleaner (IMC),

[4]Neodymium-doped yttrium aluminum garnet.

a $12m$ triangular Fabry-Perot cavity between the main laser source and the power recycle cavity [24]. It was shown [22] that the uncertainties for VCO can be reduced to 1%.

For the S5 calibration, the three method agreed within 4% [22]: "*The maximum difference between the mean value for any method and the average of the mean values for all three methods, $\bar{A}$, for any ETM, is* 3.7%."

5 Uncertainty Estimation or Error Budget

Uncertainties in the sensing scaling coefficient $\mathcal{K}_C$, are accounted for in the open loop transfer function and actuation function uncertainty. The uncertainties of the remaining quantities in the response function $A(f)$, $G_L(f)$, and $\gamma(t)$ are treated as uncorrelated.

Re-writing the response function in terms of the measured quantities with assigned uncertainties, one obtain

$$R_L(f,t) = A(f)D(f)\ \frac{1+\gamma(t)G_L(f)}{\gamma(t)G_L(f)} \tag{15}$$

and separate into magnitude and phase,

$$|R_L| = \sqrt{\left(\frac{|A|}{\gamma|G_L|}\right)^2\left[1+(\gamma|G_L|)^2+2\gamma|G_L|\cos\left(\phi_{G_L}\right)\right]} \tag{16}$$

$$\phi_{R_L} = \arctan\left(\frac{\gamma|G_L|\sin\left(\phi_A\right)+\sin\left(\phi_A-\phi_{G_L}\right)}{\gamma|G_L|\cos\left(\phi_A\right)+\cos\left(\phi_A-\phi_{G_L}\right)}\right) \tag{17}$$

such that the relative uncertainty in magnitude and absolute uncertainty in phase are

$$\begin{aligned}\left(\frac{\sigma_{|R_L|}}{|R_L|}\right)^2 &= \left(\frac{\sigma_{|A|}}{|A|}\right)^2+\Re e\{W\}^2\left(\frac{\sigma_{|G_L|}}{|G_L|}\right)^2 \\ &\quad+\ \Im m\{W\}^2\sigma^2_{\phi_{G_L}}+\Re e\{W\}^2\left(\frac{\sigma_\gamma}{\gamma}\right)^2\end{aligned} \tag{18}$$

$$\begin{aligned}\sigma^2_{\phi_{R_L}} &= \sigma^2_{\phi_A}+\Im m\{W\}^2\left(\frac{\sigma_{|G_L|}}{|G_L|}\right)^2 \\ &\quad+\ \Re e\{W\}^2\,\sigma^2_{\phi_{G_L}}+\Im m\{W\}^2\left(\frac{\sigma_\gamma}{\gamma}\right)^2,\end{aligned} \tag{19}$$

where $W \equiv 1/(1+G_L)$.

The above equations help us to visualize how the relevant magnitudes enter in the Error Budget, and how we should study them to reduce uncertainty.

For the last two LIGO science runs, S5 and S6, the magnitudes of the uncertainties were between 10% and 20% [20][21], mostly attributed to actuation scaling coefficients calibration errors. Consequently, great effort has been made to improve the MITCH and Pcal techniques. However, in S6 there was a discrepancy between this two techniques that led to an increase in the Error Budget, discrepancy that could have been understood better with the help of a third method.

Calibration requirements delivered from different GW groups to aLIGO calibration [25] can be summarized as: 10% amplitude errors, 5 degrees in phase, and $24\mu s$ in timing. In particular, it has been shown for non-spinning binary systems [7], that not only no signals would be missed because of calibration errors (using pipelines based on Bayesian factors) for calibration error meeting the above requirements, but also the effects of calibration errors on parameters estimation would be less than the statistical measurements errors.

6 VCO

In the sake of extracting as much physical information as possible from a GW detection, avoid future Error Budget increase because of calibration discrepancies, and achieve aLIGO calibration requirements, the rest of the document will center in the VCO technique, exploring possible enhancement for the calibration of second generation GW interferometers.

6.1 VCO theory: Dynamic Resonance

Malik Rakhmanov et al. [8] study the slow variation of an electromagnetic field inside a cavity. They showed that, when frequency and cavity length varies at a certain frequency f, a dynamic resonance can be acquired if the following condition holds

$$\frac{\Delta\mathcal{L}(f)}{L} = -C(f)\frac{\Delta\nu(f)}{\nu} \tag{20}$$

$$C(f) = \frac{1 - e^{-4\pi i f T}}{4\pi\ i\ f\ T} \tag{21}$$

where L is the length of the cavity, ν is the laser frequency, $\Delta\mathcal{L}(f)$ and $\Delta\nu(f)$ are the amplitudes of the variation, and $T = L/c$ is the nominal cavity transit time. For $f \ll \pi/T$, one can approximate $C(f) \approx 1$, so

$$\frac{\Delta\mathcal{L}(f)}{L} \approx -\frac{\Delta\nu(f)}{\nu} \tag{22}$$

Equation 22 is the "heart" of the VCO calibration method, showing that a controlled modulation of the interferometer's laser frequency will produce a calibrated length variation of the arm cavity. Comparing these variation with those from an actuator will lead to the calibration of the actuation scaling coefficients.

6.2 VCO: implementation

One important advantage of the VCO calibration is that doesn't need new hardware, like Pcal which is a complete auxiliary system per se. Without entering into LIGO's hardware and electronics details, let's say that LIGO utilizes a Pound-Drever-Hall (PDH) style control scheme to keep the Fabry-Perot cavities and Power recycle cavity on resonance, Figure 6. For this purpose, LIGO's main laser frequency locking servo has a VCO inside of an Acousto-Optic Modulator (AOM) driver, that creates a nominal RF at $80MHz$. This frequency changes in response to an AOM driver input signal. For S5 calibration, this system was used to create the controlled frequency variation need for the VCO calibration that led to the actuation calibration [24]. The same scheme could be repeated with a better sideband-to-carrier measurement which will enhance the VCO uncertainty, giving an independent actuation calibration improving the uncertainty of the complete calibration.

7 Second Generation GW detectors: aLIGO

The complexity of aLIGO's interferometer introduces more degrees of freedom. A new framework called Arm Length Stabilization (ALS) system [26] is being implemented in order to stabilize each Fabry-Perot cavity independently, in order to lock the complete interferometer. The system uses green auxiliary lasers to lock each arm separately, generating new differential and common arm length modes signals, Figure 7. Each green ALS laser also uses a PDH style error signal, which allows the possibility of using them for a VCO calibration of the actuation function. The implementation of green VCO will mend the SNR problem, since will avoid the IMC path, and also could led to a science mode implementation of the VCO.

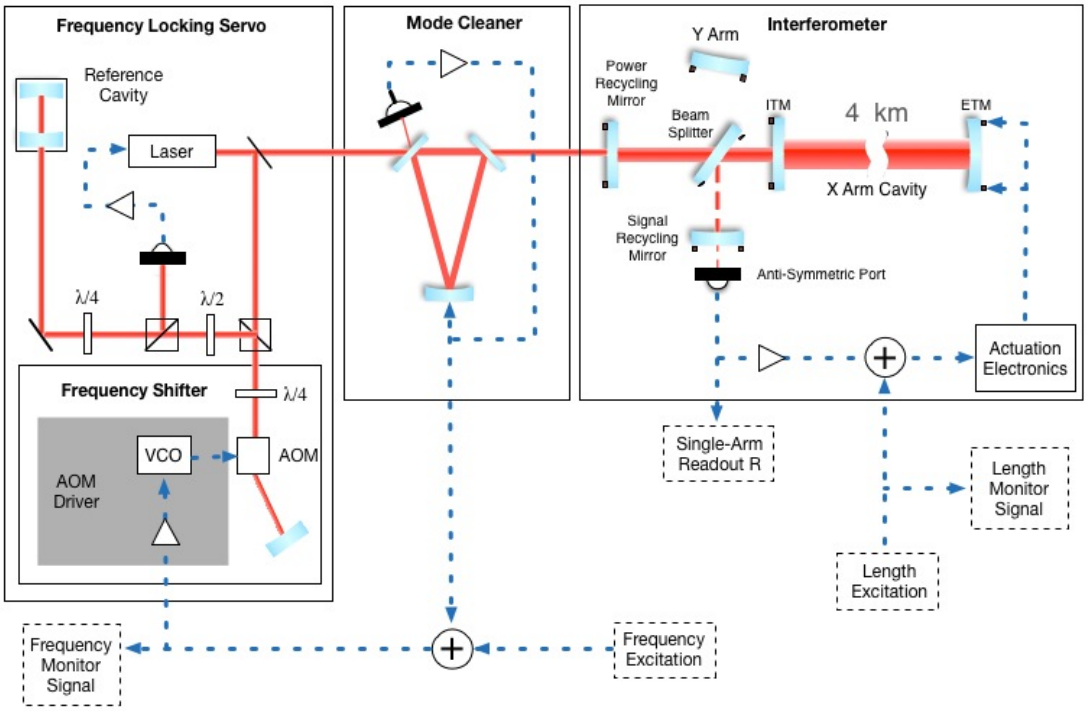

Figure 6: Schematic of the experimental setup used to calibrate ETM actuators.

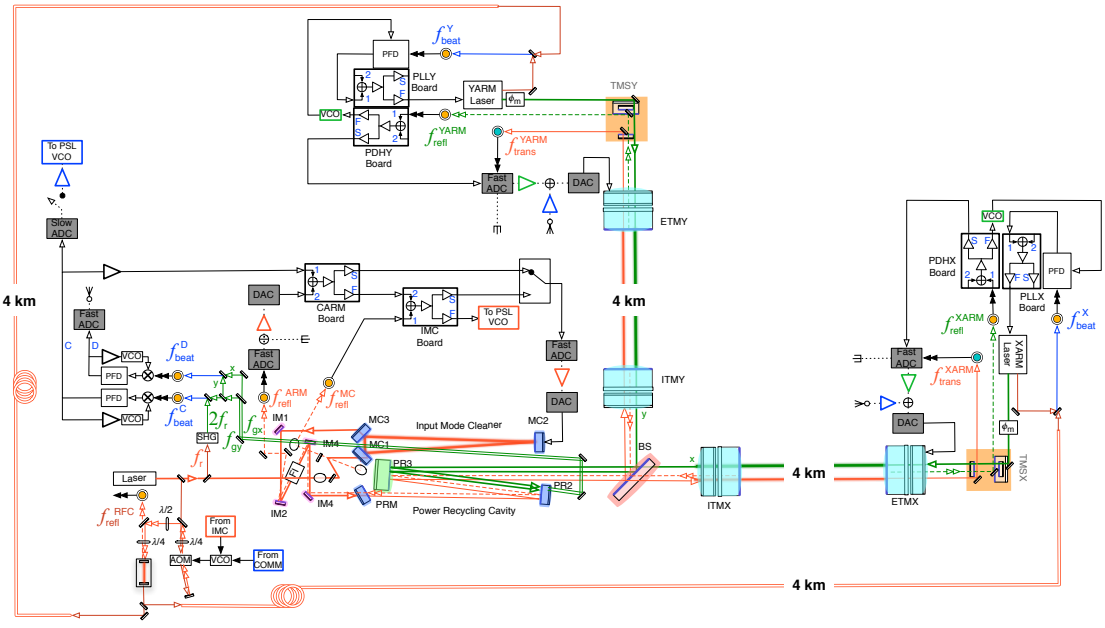

Figure 7: aLIGO ALS Electro-Optical Control Schematic. (*Credit: J. Kissel*)

8 Proposal

In order to extract as much astrophysical information as possible from a GW detection, all possible improvements in the calibration should be explored, developed and implemented. The

VCO calibration is a complete independent calibration method, which relies on laser frequency variation inside a Fabry-Perot cavity. It does not need new hardware, neither sequential measurements in different interferometer/electronics configurations. Also, because of its nature, is the only calibration method that doesn't applies forces on ETMs, which allow the study of elastic deformation [27], in particular at at high frequencies [28]. The method was applied successfully during S5. Nevertheless, aLIGO open new possibilities to achieve better accuracies, and maybe, a simpler calibration scheme for this method.

The VCO S5 calibration had an uncertainty of 0.8% [24]. Most of this error is attributed to two sources. One is the sideband-to-carrier measurement, which can be improved. The other is the low SNR of the VCO signal, product of the complexity of the interferometer, which uses a IMC. Avoiding the IMC will lead to a better SNR, and hence a better uncertainty. The use of ALS green lasers, not only mend the SNR/IMC problem, but also could lead to a VCO calibration during science mode. What is most important, a third calibration method could mend the inflation of the Error Budget due to calibration discrepancies between MITCH and Pcal.

At this point, it is important to highlight that precise calibration of the interferometers allows less accuracy in templates used for GW searches, which is an advantage for first detections.

The VCO calibration, not only could improve the accuracy, but also will give confidence to second generation GW detectors calibration.

Is estimated for middle next year, aLIGO will be working at its nominal configuration. That give me the sufficient time to study all the problems involved in the implementation of the VCO. New lasers, new actuators, new optics with new coating, and a myriad of new electronics/hardware to be tested will occupied the major part of the work. Finally, the ability of attain, reliable calibration errors would lead not only to the first GW detection, but also to a new window to observe astrophysical events.

References

[1] A. Bauswein, H. T. Janka, 2011, *Measuring neutron-star properties via gravitational waves from neutron-star mergers*. arXiv:1106.1616 [astro-ph.SR].

[2] Ilya Mande, Richard O'Shaughnessy, 2010, *Compact Binary Coalescences in the Band of Ground-based Gravitational-Wave Detectors*. arXiv:0912.1074 [astro-ph.HE].

[3] Chandra Kant Mishra, K. G. Arun, Bala R. Iyer, B. S. Sathyaprakash, 2010, *Parametrized tests of post-Newtonian theory using Advanced LIGO and Einstein Telescope*. arXiv:1005.0304 [gr-qc].

[4] Walter Del Pozzo, John Veitch, Alberto Vecchio, 2011, *Testing General Relativity using Bayesian model selection: Applications to observations of gravitational waves from compact binary systems*. arXiv:1101.1391 [gr-qc].

[5] Walter Del Pozzo, et al., 2012, *Inference of the cosmological parameters from gravitational waves: application to second generation interferometers*. arXiv:1108.1317 [astro-ph.CO].

[6] Stephen R. Taylor, Jonathan R. Gair, Ilya Mandel, 2012, *Hubble without the Hubble: Cosmology using advanced gravitational-wave detectors alone*. arXiv:1108.5161 [gr-qc].

[7] Salvatore Vitale, et al., 2012, *Effect of calibration errors on Bayesian parameter estimation for gravitational wave signals from inspiral binary systems in the advanced detectors era*. arXiv:1111.3044 [gr-qc].

[8] M. Rakhmanov, et. al., 2001, *Dynamic Resonance of Light in Fabry-Perot Cavities*. arXiv:physics/0110061 [physics.optics].

[9] A. Einstein 1987, *Approximative integration of the field equations of gravitation*, The Collected Papers of Albert Einstein, Princeton University Press pp. 201-210.

[10] J. Taylor and J. Weisberg 1982, *A new test of general relativity: gravitational radiation and the binary pulsar PSR 1913+16*, The Astrophysical Journal, vol. **253**, pp. 908-920.

[11] BICEP2 collaboration, 2014, http://www.cfa.harvard.edu/news/2014-05.

[12] J. Weber, 1960, *Detection and generation of gravitational waves*, Physical Review, vol. **117**, pp. 306-313.

[13] J. Weber, 1961, *General Relativity and Gravitational Waves*. New York: Interscience Publishers, Inc.

[14] J. Weber, 1969, *Evidence for discovery of gravitational radiation*, Physical Review Letters, vol. **22**, pp. 1320-1324.

[15] M. Gertsenshtein and V. Pustovoit, 1963, *On the detection of low frequency gravitational waves*, Soviet Physics JETP, vol. **16**, pp. 433-435.

[16] J. Weber. unpublished.

[17] R. Weiss, 1972, *Electromagnetically coupled broadband gravitational antenna*, Quarterly Progress Report of the Research Laboratory of Electronics of the Massachusetts Institute of Technology, vol. **105**, pp. 54-76.

[18] G. Moss, L. Miller, and R. Forward, 1971, *Photon-noise-limited laser transducer for gravitational antenna*, Applied Optics, vol. **10**, pp. 2495-2498.

[19] J. Kissel, *Hierarchical Control Theory for Advanced LIGO*, `LIGO DCC-T1000242`, `LIGO DCC-G1200692`

[20] LIGO Scientific Collaboration, 2010, *Calibration of the LIGO Gravitational Wave Detectors in the Fifth Science Run.* arXiv:1007.3973 [gr-qc].

[21] Imre Bartos, et al., 2011, *Frequency Domain Calibration Error Budget for LIGO in S6.* LIGO Document DCC-T1100071.

[22] Goetz E, et al. 2010 *Accurate calibration of test mass displacement in the LIGO interferometers.* Class. Quantum Grav. **27** (2010) 084024 (11pp)

[23] Goetz E, et al. 2009, *Precise calibration of LIGO test mass actuators using photon radiation pressure,Class. Quantum Grav.* **26** 245011.

[24] Goetz E, et al. 2010 *Calibration of the LIGO displacement actuators via laser frequency modulation.* Class. Quantum Grav. **27** 215001.

[25] J Betzwieser, et al., 2013 *Calibration Uncertainty Budget Requirements for early aLIGO*, LIGO DCC-T1300950

[26] Matt Evans, et al., 2010 *Advanced LIGO Arm Length Stabilisation System Design*, LIGO DCC-T0900144

[27] S Hild, et al., 2007 *Photon-pressure-induced test mass deformation in gravitational-wave detectors.* Class. Quantum Grav. **24** 5681

[28] P Daveloza, et al 2012, *Controlling calibration errors in gravitational-wave detectors by precise location of calibration forces* , J. Phys.: Conf. Ser. **363** 012007